

## Large Reaction Rate Enhancement in Formation of Ultrathin AuSi Eutectic Layers

Tyler S. Matthews,<sup>1,2</sup> Carolyn Sawyer,<sup>1,2</sup> D. Frank Ogletree,<sup>3</sup> Zuzanna Liliental-Weber,<sup>2</sup>  
Daryl C. Chrzan,<sup>1,2</sup> and Junqiao Wu<sup>1,2,\*</sup>

<sup>1</sup>Department of Materials Science & Engineering, University of California, Berkeley, California 94720, USA

<sup>2</sup>Materials Sciences Division, Lawrence Berkeley National Laboratory, Berkeley, California 94720 USA

<sup>3</sup>The Molecular Foundry, Lawrence Berkeley National Laboratory, Berkeley, California 94720 USA

(Received 28 November 2011; published 1 March 2012)

Metal-semiconductor eutectic liquids play a key role in both the fundamental understanding of atomic interactions and nanoscale synthesis and catalysis. At reduced sizes they exhibit properties distinct from the bulk. In this work we show an unusual effect that the formation of AuSi eutectic liquid layers is much easier for smaller thicknesses. The alloying reaction rate is enhanced by over 20 times when the thickness is reduced from 300 to 20 nm. The strong enhancement is attributed to a strain-induced increase in the chemical potential of the solid layer prior to the alloying reaction.

DOI: 10.1103/PhysRevLett.108.096102

PACS numbers: 68.08.De, 64.70.D-, 64.75.Jk, 68.35.Fx

Metal-semiconductor eutectic alloys are widely used for metal-catalyzed semiconductor synthesis, nanomaterial assembly, and interface bonding. Surprising new physical effects were recently discovered at the surface or reduced sizes of these metallic liquids. For the  $\text{Au}_{0.81}\text{Si}_{0.19}$  eutectic formed at  $T_{\text{eut}} = 363^\circ\text{C}$ , for example, a Si-enriched surface layering was discovered [1,2]. The surface Si enrichment is understandable considering the lower surface tension of liquid Si than Au [2], while the surface layering mechanism is still in debate [3–5]. Other interesting effects have also been observed or suggested in eutectic liquids such as substrate-enhanced supercooling [6] and eutectic temperature modification in nanostructures [7]. These remarkable surface, interface and size effects challenge our fundamental understanding of atomic interactions in metallic liquids.

The majority of these experimental investigations were performed in *static* states. Elucidation of the physical mechanism underlying these unusual phenomena, however, requires probing of the *dynamic* eutectic formation. Atomic diffusion and the alloying reactions are fundamental steps governing the dynamic process. It was reported, for example, that the diffusivity of Au in bulk AuSi eutectic is 1 order of magnitude higher than in pure Au at the same temperature [8,9]. For spreading of a Au monolayer on solid Si, the Au diffusion was found to be too fast to be measureable [10]. However, probing atomic diffusion and alloying reactions in *nanoscale* eutectic liquids is very difficult due to Rayleigh instability of ultrathin liquids, the small time and size scales involved, as well as sensitivity of the processes to boundary conditions [11].

In this work, we show that for Au layers connected to a Si reservoir, the formation of AuSi eutectic liquids is much easier for thinner Au layers. The alloying reaction rate to form the eutectic is enhanced for more than 20 times when the Au layer thickness is reduced from 300 to 20 nm. In our experiments, *in situ* probing of the formation of thin

eutectic layers is enabled by designing a self-limited diffusion-alloying process.

Thin layers of Au were deposited onto Si (100) substrates using electron beam evaporation. Prior to the Au deposition, the native oxide of the Si was *not* removed and the samples had not been thermally treated. The samples were annealed in vacuum at temperatures near  $600^\circ\text{C}$  for several minutes, followed by natural cooling back to room temperature. At the high temperatures, the AuSi eutectic forms when Si atoms diffuse out of the Si reservoir via weak spots in the native oxide, while everywhere else the native oxide serves as a diffusion barrier isolating the film from the reservoir. In this way, the Au overlayer is fully converted into a thin AuSi eutectic layer with a thickness that is uniform and determined by the thickness of the predeposited Au. On the surface we observed peculiar circular features with a square at the center of each circle, which are ruptured thin layers of eutectic liquid. By analyzing the geometries and *in situ* monitoring the formation speed of these features, we were able to calculate the atomic diffusion and alloying rates in the eutectic for different eutectic thicknesses. A typical scanning electron microscopy (SEM) image of an annealed sample is given in Fig. 1. The ruptured zones appear randomly across the entire surface [Fig. 1(a)] with varying radii and central square dimension. We refer to these zones as denuded zones (DZs) as they are devoid of film material. In contrast, the areas outside the DZs feature irregularly ruptured material. The central squares have right angles at the corners [Fig. 1(c)], with extremely sharp edges parallel to  $\langle 110 \rangle$  and to all other squares across the entire sample, indicating epitaxial registration with the bulk Si (100) substrate. DZs were observed for all deposited Au film thicknesses ranging from  $\sim 12$  nm to 300 nm, and the minimum annealing temperature required for DZs to appear was  $\sim 600^\circ\text{C}$ .

The rapid formation and rupture process of the DZs was observed in real-time (see video in supplemental material

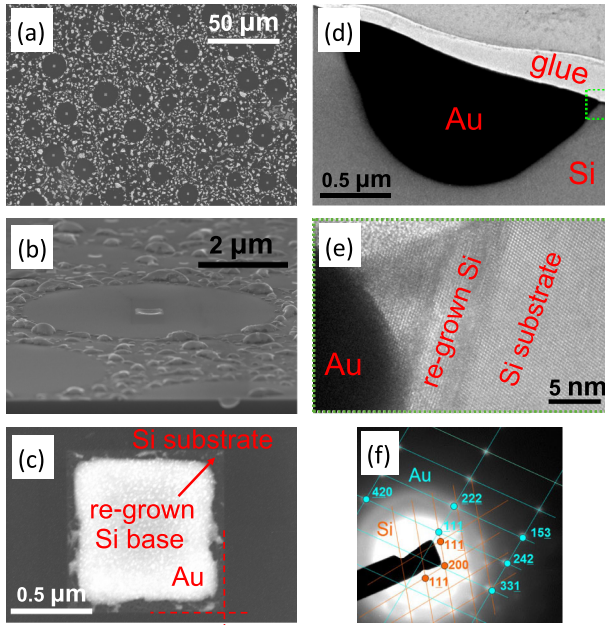


FIG. 1 (color online). (a) An SEM image of the formed AuSi microfeatures, (b) Tilted view of a denuded zone (DZ) with a depressed square in the center. (c) The central square has an extremely sharp and regular square base (regrown Si) as highlighted by dashed lines, and less regular Au accumulated in the center. (d) Low-resolution cross-sectional TEM image of a single AuSi center square. (e) High-resolution TEM image of the highlighted area in (d). (f) Selected area electron diffraction confirming segregated crystalline phases of Au and Si. The zone axis is Au  $[123]$  and Si  $[011]$ .

[12]) utilizing an *in situ* SEM. Immediately prior to the rupture event, a dark contrast circle (called “grey zone”, GZ) was observed to rapidly form and expand to the area that was to become a DZ. After the rupture the entire central square was completely filled with a AuSi alloy which, during cooling, segregated into pure Au and Si.

Cross-sectional transmission electron microscope (TEM) samples were prepared by cleaving the Si substrate along its (011) plane, revealing an inverted pyramid shape [Fig. 1(d)]. The angle between the Si substrate surface and the interfacial Si region was determined to be  $\sim 55^\circ$ , indicating the pyramid facets correspond to the  $\{111\}$  planes in Si.

A schematic side view of the central pyramid and surrounding DZ prior to rupture is depicted in Fig. 2(a). Here we assume that an opening exists within the native oxide layer in the center that serves as a narrow channel for rapid interdiffusion of Au from the overlayer to the wafer and Si from the wafer to the overlayer. A geometric relationship between the side length of the central square ( $a$ ) and the surrounding DZ radius ( $R$ ) can be readily derived from mass conservation. We consider the DZ area immediately prior to the rupturing event as a “disc” of alloyed material with composition  $\text{Au}_f\text{Si}_{1-f}$ , where  $f$  is the mole fraction

of Au in the alloy, which is assumed to be approximately equal and uniform in the disc and pyramid. Mass conservation leads to the following relationship between  $R$  and  $a$ ,

$$R = \sqrt{\tilde{f}/[3\sqrt{2}\pi(1-\tilde{f})d]}a^{3/2}, \quad (1)$$

where  $d$  is the disc thickness, and  $\tilde{f}$  is the volume fraction of Au and is related to its mole fraction  $f$  through the density of Si and Au. Equation (1) predicts that  $R$  scales linearly to  $a^{3/2}$ , where the coefficient depends on  $f$  and scales linearly with  $d^{-1/2}$ . A plot of  $R$  versus  $a^{3/2}$  for various film thicknesses is given in Fig. 2(d), which shows a series of straight lines converging precisely to  $R = 0$  at  $a = 0$ . A plot of the slope ( $c$ ) of lines in Fig. 2(d) as a function of  $d^{-1/2}$  is shown in Fig. 2(e). It can be seen that again the linear dependence is excellent, and the line also extrapolates to  $c = 0$  at  $d^{-1/2} = 0$ . The slope of the linear dependence in Fig. 2(e) yields a Au volume fraction of  $\tilde{f} = 0.78 \pm 0.02$ , corresponding to  $f = 0.81 \pm 0.02$ , which is precisely the Au-Si eutectic mole fraction,  $f_{\text{eut}}$ , as indicated on the AuSi phase diagram in Fig. 2(c). The excellent, simultaneous fitting to Eq. (1) for all Au layer thicknesses in turn justifies our assumption that immediately prior to the rupturing event, the GZ was comprised of a nearly homogeneous  $\text{Au}_f\text{Si}_{1-f}$  eutectic liquid alloy.

As the temperature is increased from room temperature, the native oxide layer weakens. It is known that the mechanical properties of  $\text{SiO}_2$  change dramatically at  $\sim 600^\circ\text{C}$  [13]. We speculate that at  $\sim 600^\circ\text{C}$ , small holes rapidly open in the native oxide layer, most likely around preexisting pinholes, an effect previously observed in an-

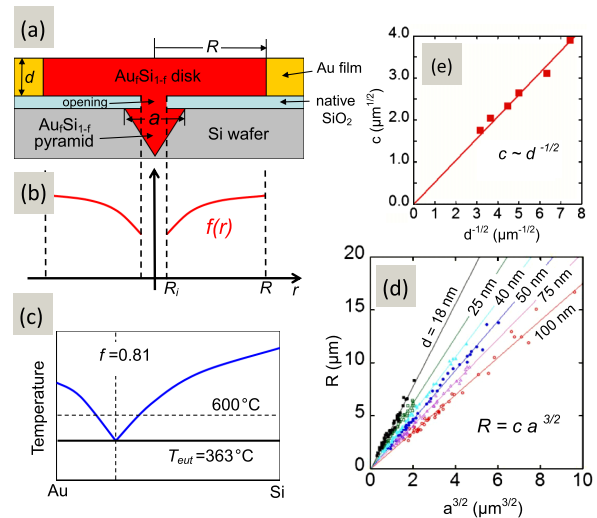


FIG. 2 (color online). (a) A side-view schematic of the structure immediately prior to rupture. (b) A schematic of Au mole fraction as a function of radial position. (c) Au-Si phase diagram. (d) Scaling relationship between the denuded circle radius  $R$  and the center square size  $a$ . The lines are fits to the equation shown in the figure. (e) The coefficient  $c$  as a function of the Au film thickness  $d$ . A linear fit gives the Au molar fraction  $f$ .

nealing Pt films on Si with a native oxide present [14]. These openings provide small interfacial regions where Au and Si come in direct contact. They interdiffuse across this interface, leading to the formation of the eutectic liquid and driving the eutectic disc and pyramid to expand. We note that strain- or temperature-driven convection is expected to be weak in such thin, viscous liquids and will be ignored in our discussion. After the eutectic discs form, they tend to rupture driven by the high AuSi/SiO<sub>2</sub> interface energy. This rupturing is a conventional liquid film dewetting process. Generally speaking, a liquid film ruptures due to instability with respect to thickness fluctuations of lateral wavelengths larger than a critical length,  $\lambda_c$  [15,16]. Perturbation with wavelengths longer than  $\lambda_c$  is possible only in liquid films with a lateral size ( $\sim 2R$  in our case) larger than  $\lambda_c$ . The rupture completely drains the eutectic discs and forms empty DZs [Fig. 3(a)]. This threshold and the fluctuation-driven nature of the dewetting explain the fact that the final  $R$  has a broad distribution with a finite minimum for all thicknesses, as can be seen in Fig. 2(d).

We evaluate the dynamic process by analyzing Si diffusion in the AuSi eutectic disc from the central opening (at radius  $r = R_i < a$ ) to the perimeter ( $r = R$ ). This is a

standard diffusion-reaction process similar to that in the chemical vapor deposition of films. Solving the two-dimensional diffusion equation gives the radial dependence of the Si fraction [10],

$$f_{\text{Si}}(r) = [f_{\text{Si}}(R) - f_{\text{Si}}(R_i)] \frac{\ln(r/R_i)}{\ln(R/R_i)} + f_{\text{Si}}(R_i). \quad (2)$$

The fraction of Au is  $f(r) = 1 - f_{\text{Si}}(r)$ . While the eutectic liquid can be expected to support Fickian diffusion, it becomes necessary to analyze diffusion in terms of chemical potential gradients, rather than liquid composition, in the presence of both liquid and solid. Assuming an ideal solution behavior for the liquid,  $f(r) = \exp[(\mu(r) - \mu_0)/k_B T]$ , the Au diffusion flux at the disc perimeter (reaction front  $r = R$ ) will be

$$\begin{aligned} J_{\text{diffuse}}(R) &= -D_{\text{Au}} \left. \frac{df(r)}{dr} \right|_{r=R} \\ &= -\frac{D_{\text{Au}}}{R \ln(R/R_i)} \left[ \exp\left(\frac{\mu(R) - \mu_0}{k_B T}\right) - \exp\left(\frac{\mu_i - \mu_0}{k_B T}\right) \right], \end{aligned} \quad (3)$$

where  $\mu$  is the chemical potential of Au in the liquid alloy,  $\mu_0$  is an arbitrary reference value, and  $\mu_i \equiv \mu(R_i)$ . The alloying flux for the reaction  $\text{Si} + \text{Au} \rightarrow \text{Au}_f\text{Si}_{1-f}$  at  $r = R$  is

$$J_{\text{alloy}}(R) = M[\mu(R) - \mu_{\text{solid}}], \quad (4)$$

where  $M$  is the mobility of the AuSi/Au interface, and  $\mu_{\text{solid}}$  is the chemical potential of Au in the solid phase. Equating  $J_{\text{alloy}}$  and  $J_{\text{diffuse}}$  at  $r = R$  gives

$$\begin{aligned} -\frac{D_{\text{Au}}}{R \ln(R/R_i)} \left[ \exp\left(\frac{\mu(R) - \mu_0}{k_B T}\right) - \exp\left(\frac{\mu_i - \mu_0}{k_B T}\right) \right] \\ = M[\mu(R) - \mu_{\text{solid}}]. \end{aligned} \quad (5)$$

Taylor-expanding the exponentials to the first order, this can be solved for  $\mu(R)$ , and substituted into Eq. (4) to get the radial expansion speed of the reaction front,

$$\frac{dR}{dt} = -J_{\text{alloy}}(R) = \frac{M(\mu_{\text{solid}} - \mu_i)}{1 + (Mk_B T/D_{\text{Au}})R \ln(R/R_i)}. \quad (6)$$

Equation (6) has a solution given by

$$\begin{aligned} R(t) + \frac{Mk_B T}{2D_{\text{Au}}} R^2(t) \left[ \ln \frac{R(t)}{R_i} - \frac{1}{2} \right] \\ = M(\mu_{\text{solid}} - \mu_i)(t - t_0). \end{aligned} \quad (7)$$

This can be used to fit the measured  $R(t)$  and obtain the two parameters, namely, the effective diffusivity  $D_{\text{Au}}/M$  and the linear reaction rate  $M\Delta\mu \equiv M(\mu_{\text{solid}} - \mu_i)$ . If

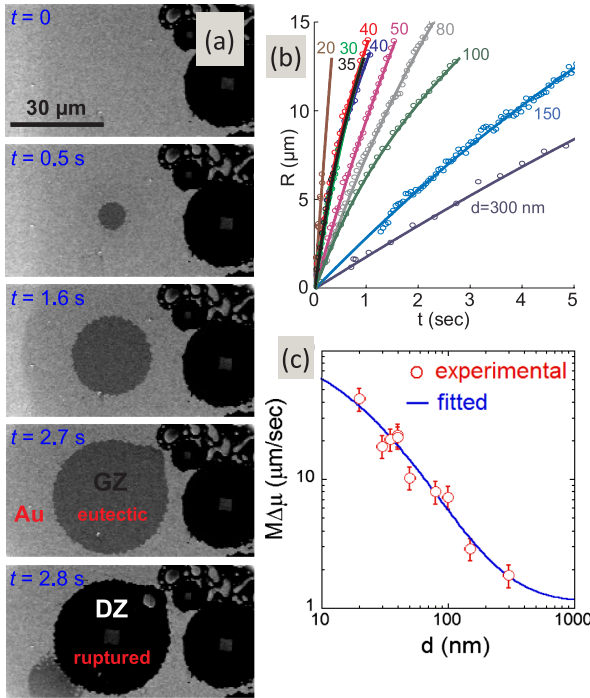


FIG. 3 (color online). (a) Rapid formation of a DZ through an expanding gray zone (GZ), imaged at 600 °C using *in situ* SEM on a sample with Au thickness of 100 nm. (b) The GZ radius evolving as a function of time for different Au thicknesses  $d$ . The lines are fits of Eq. (7). The agreement between the two 40 nm films shows the good reproducibility of the data. (c) Measured and fitted [using Eq. (8)] reaction rate as a function of Au thickness.

$D_{\text{Au}}/M \gg k_B TR \ln(R/R_i)$ , the process is reaction limited and  $R(t)$  becomes linear in  $t$ , while if  $D_{\text{Au}}/M \ll k_B TR \ln(R/R_i)$ , the process becomes diffusion limited and  $R(t) \propto \sqrt{t}$ .

Figure 3(b) shows experimentally measured  $R(t)$  for a range of film thicknesses  $d$ , with the fits using Eq. (7). It can be seen that the nonlinearity of all  $R(t)$  is relatively weak, indicating that the atomic diffusion is relatively fast and the alloying reaction limits the expansion speed of the GZs, at least during the initial stages of growth. Therefore, the atomic fraction  $f(r)$  is expected to be nearly constant for all positions  $r \leq R$ . More importantly,  $R(t)$  grows much faster for thinner  $d$ . The fitted  $M\Delta\mu$  is shown as a function of  $d$  in Fig. 3(c), which shows 23 times increase between the thickest and thinnest films measured. On the other hand, while  $D_{\text{Au}}/M$  varies between samples, there is no clear thickness dependence, probably attributed to large errors in fitting the weak nonlinearity in the  $R(t)$  curves.

It has been established that when metal films are evaporated, they tend to be tensile strained by both thermal expansion mismatch with the substrate and collapse of voids among the grains [17]. Metal films may relieve this stress via plastic deformation, specifically by glide of dislocations, such that the stress remaining in the as-grown film will be the flow stress. The surface of a thin film acts as a barrier to dislocation glide, leading to a  $1/d$  dependence in the flow stress [18–20]; however, this  $1/d$  dependence will be limited for ultrathin films by either the applied stress being lower than the yield stress, or other mechanisms associated with plasticity [18]. This capped  $1/d$  dependence can be modeled in a simple way by an equation of the form  $\sigma \propto 1/(1 + d/d_0)$ , where  $\sigma$  is the residual stress and  $d_0$  is a characteristic film thickness below which the stress is capped. The chemical potential of the solid Au film will be increased by the stress by an amount equal to  $V_m \sigma^2 / 2Y$ , where  $V_m$  is the atomic volume and  $Y$  is the elastic modulus of Au. The liquid eutectic film, on the other hand, is able to relax the strain completely. Therefore, the reaction rate  $M\Delta\mu$  fitted from Eq. (7) is expected to follow

$$M\Delta\mu(d) = M\Delta\mu(\infty) + M \frac{V_m \sigma_0^2}{2Y(1 + d/d_0)^2}. \quad (8)$$

Equation (8) is fitted to the experimental data in Fig. 3(c) and we obtain  $d_0 = 19$  nm,  $MV_m \sigma_0^2 / 2Y = 164 \mu\text{m/s}$ , and  $M\Delta\mu(\infty) = 1.2 \mu\text{m/s}$ .

Leung *et al.* [18] observed a flow stress dependence  $\sigma \approx 0.14$  GPa  $\mu\text{m}/d$  for thick Au films; using this value,  $\sigma_0$  is determined to be 7.4 GPa. The elastic modulus of solid Au at 600 °C is  $Y \approx 60$  GPa [21]. This leads to an interface mobility of  $M = 3.6 \times 10^{-13}$  m/s Pa. While the interface mobility of Au is not tabulated in the literature, Trautt *et al.* [22] have found the grain boundary interface mobility in high-temperature (930 °C) Au to be on the order of  $10^{-8}$  m/s Pa; the orders of magnitude difference may be

explained by the much lower temperature used in the current experiments, since interface motion is a thermally activated process [23], and by the difficulty of incorporating the second species (Si). Combining this value of  $M$  with the other fitting parameter  $D_{\text{Au}}/M$ ,  $D_{\text{Au}}$  is found to be between  $4 \times 10^3$  and  $5 \times 10^4 \mu\text{m}^2/\text{s}$ , which is approximately on the same order as the reported  $2 \times 10^3 \mu\text{m}^2/\text{s}$  of Au diffusing in bulk AuSi at 600 °C [9]. We note that the highest observed stress occurs in the 20 nm film and is estimated to be  $\sim 3.6$  GPa. An upper bound on the stress is provided by the ideal strength. The ideal strength of bulk Au has been calculated to be between 1.5 GPa [23] and 4.8 GPa [24] depending on crystallinity and orientation. Au nanowires a few to tens of nm in diameter have shown yield strengths up to 4 GPa [25] or 8 GPa [24]. Nanoindentation experiments also have shown yield stresses in Au as high as 7.8 GPa [26]. These results compare favorably with the fitted stress in the ultrathin films studied in this work.

In summary, at the reaction front of the AuSi eutectic layer, the driving force of the reaction is rapidly increased when the layer thickness is reduced below 100 nm, following a simple scaling relationship with the thickness. This effect is attributed to strain effects in the solid Au layer that boosts the chemical driving force of the reaction. The thickness dominated alloying reaction may provide new routes for nanoscale materials engineering and processing.

This work was supported by a NSF CAREER Award under the Grant No. DMR-1055938. Portions of this work (*in situ* SEM) were performed as user projects at the Molecular Foundry, Lawrence Berkeley National Laboratory. The theoretical analysis part was supported by the Office of Science, Office of Basic Energy Sciences, of the U.S. Department of Energy under Contract No. DE-AC02-05CH11231. We thank Professor Peter Voorhees, Professor Mark Asta, Dr. Shaul Aloni, and Dr. Andreas Schmid for useful discussions and Ed Wong for technical assistance. T.S.M. acknowledges a Jane Lewis Fellowship from U.C. Berkeley.

\*wuj@berkeley.edu

- [1] O. G. Shpyrko *et al.*, *Science* **313**, 77 (2006).
- [2] O. G. Shpyrko *et al.*, *Phys. Rev. B* **76**, 245436 (2007).
- [3] S. Mechler *et al.*, *Phys. Rev. Lett.* **105**, 186101 (2010).
- [4] S. H. Lee *et al.*, *J. Phys. Chem. C* **114**, 3037 (2010).
- [5] V. Halka *et al.*, *J. Phys. Condens. Matter* **20**, 355007 (2008).
- [6] T. U. Schulli *et al.*, *Nature (London)* **464**, 1174 (2010).
- [7] H. Adhikari *et al.*, *Nano Lett.* **6**, 318 (2006).
- [8] A. Pasturel *et al.*, *Phys. Rev. B* **81**, 140202 (2010).
- [9] A. Bruson *et al.*, *J. Appl. Phys.* **53**, 3616 (1982).
- [10] N. Ferralis *et al.*, *Phys. Rev. Lett.* **103**, 256102 (2009).
- [11] V. C. Holmberg *et al.*, *Nano Lett.* **11**, 3803 (2011).
- [12] See Supplemental Material at <http://link.aps.org/supplemental/10.1103/PhysRevLett.108.096102> for details and a video.

- 
- [13] D. A. McGraw, *J. Am. Ceram. Soc.* **35**, 22 (1952).  
[14] E. Conforto *et al.*, *Philos. Mag. A* **81**, 61 (2001).  
[15] A. Vrij, *Discuss. Faraday Soc.* **42**, 23 (1966).  
[16] A. Sharma and R. Khanna, *Phys. Rev. Lett.* **81**, 3463 (1998).  
[17] D.L. Smith, *Thin Film Deposition: Principles and Practice* (McGraw-Hill, New York, 1995).  
[18] O. S. Leung *et al.*, *J. Appl. Phys.* **88**, 1389 (2000).  
[19] M.J. Kobrinsky *et al.*, *Appl. Phys. Lett.* **73**, 2429 (1998).  
[20] C. V. Thompson, *J. Mater. Res.* **8**, 237 (1993).  
[21] S. M. Collard, Ph.D. thesis, Rice University, 1991.  
[22] W. Grünwald *et al.*, *Acta Metall.* **18**, 217 (1970).  
[23] K. Gall *et al.*, *Nano Lett.* **4**, 2431 (2004).  
[24] B. Wu *et al.*, *Nature Mater.* **4**, 525 (2005).  
[25] N. Agraït, G. Rubio, and S. Vieira, *Phys. Rev. Lett.* **74**, 3995 (1995).  
[26] J.D. Kiely and J.E. Houston, *Phys. Rev. B* **57**, 12 588 (1998).

Supplemental material to

**“Large Reaction Rate Enhancement in Formation of Ultra-Thin AuSi Eutectic Layers”, T. Matthews et al.**

1. Experimental details.

Control samples without the native oxide were prepared using an HF etch immediately before the Au deposition, and these samples did not exhibit the circular features upon annealing. All results presented in the main text are for samples with the native oxide still present.

Monitoring at higher time-resolution to more accurately determine zone expansion rates was accomplished using a custom-built apparatus consisting of a vacuum chamber with a resistive heating stage and optically transparent window. The samples were placed inside the chamber directly on top of the heating stage and covered with a foil cap to reflect radiative heat. The chamber was pumped down to  $\sim 10^{-3}$  Torr and the stage was slowly heated ( $< 1$  °C per minute) to 600 °C using a DC power supply operated under current control. A microscope with a digital video camera was then used to capture video sequences during annealing.

Diffusion rate analysis was performed by extracting image sequences from the video corresponding to individual DZ formation events. The zone diameters in the resultant images were calibrated by first capturing video sequences of a section of the sample with photolithography patterned lines having a width of 10  $\mu\text{m}$ . The GZ expansion rate was then measured from the first video frame showing the GZ emerging until the final event forming the DZ.

2. The presence of the ultra-thin ( $\sim 2$  nm) native oxide layer is critical for the formation of the DZs: without the oxide layer acting as a diffusion barrier, the eutectic would form simultaneously everywhere and then rupture into random structures, as seen after annealing Au-coated Si wafers where the native oxide was etched prior to Au deposition (Fig.S1). On the other hand, if the oxide layer is too thick (thicker than the Au layer), the opening would be deeper than the Au layer thickness, such that a continuous interdiffusion cannot be ensured at the opening.

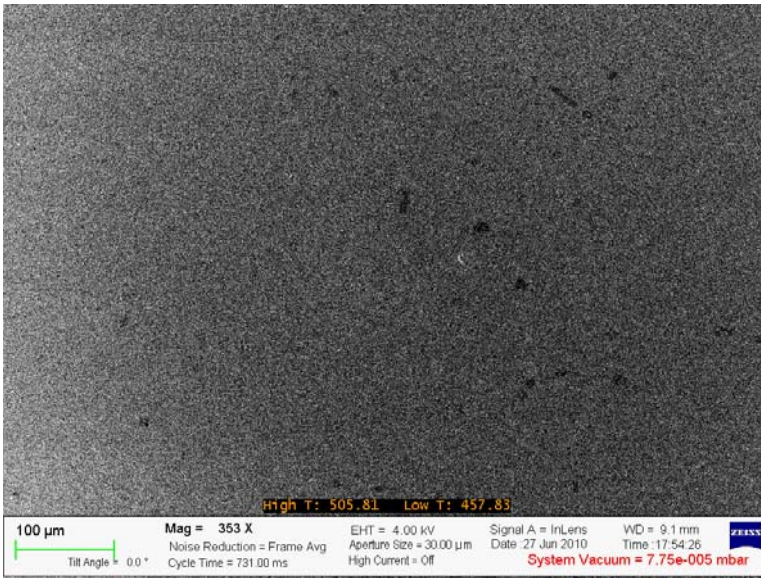


*Fig.S1. A SEM image of annealed sample on HF-treated Si wafer showing no formation of DZs. The Au thickness is 100 nm.*

### 3. Overlapped DZs.

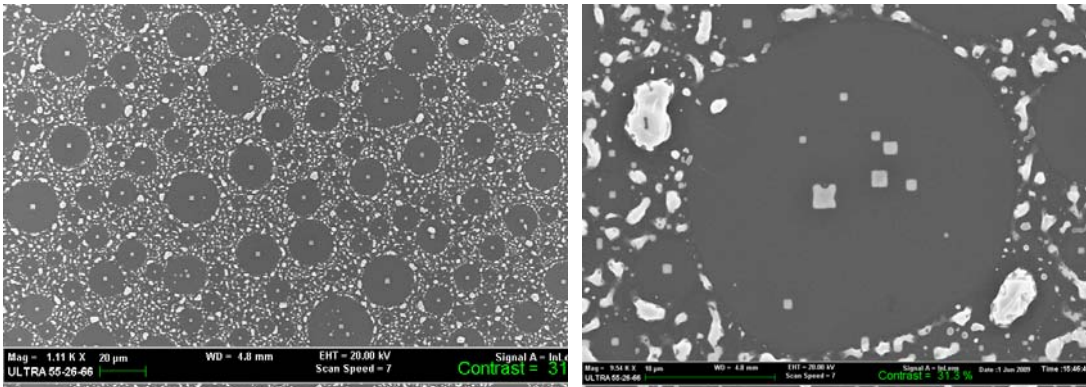


*Fig.S2. SEM images of annealed sample showing accidentally overlapped DZs, namely, non-perfect circles with multiple squares inside each circle. Here the Au thickness is 30 nm. The DZ overlapping is less common for thinner Au thicknesses.*

4. An interesting case worthy of discussion is that of the 10 nm thick Au films, the lowest thickness where DZs could form. After annealing films with a Au thickness below 10 nm, only irregular islands formed across the entire surface, similar to those outside circular DZs in thicker films. This is explained by the rupture of the Au layer itself before the AuSi eutectic can possibly form, which is because of the strong melting point suppression of the sub-10 nm thick Au layer. At precisely 10 nm, however, non-circular zones formed which are covered with a fine network composed of nanoscale AuSi filaments and openings (Fig. S3). These features were stable at temperatures exceeding 650 °C. It is possible that at such low thickness, the dewetting dynamics of liquid AuSi eutectic layer

favors a localized rupture, rather than an extended rupture that drains the entire eutectic and creates a DZ as in higher thicknesses.

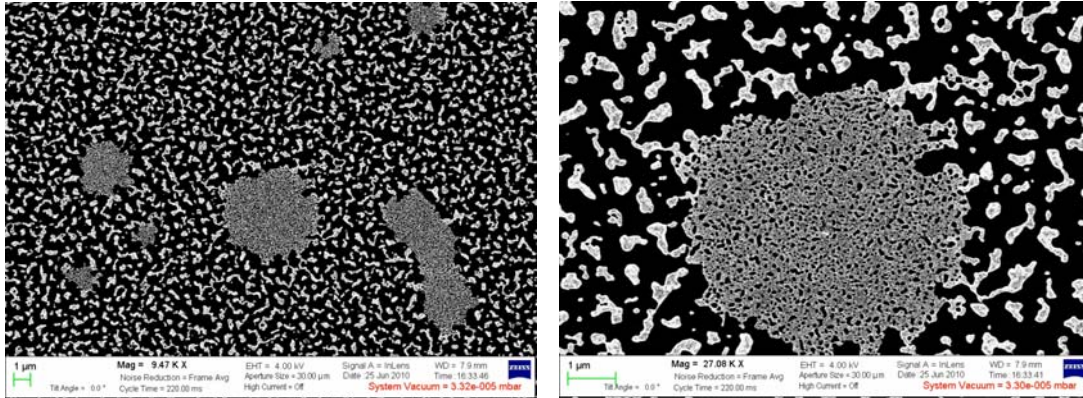


*Fig. S3. When the Au layer is 10nm, upon annealing non-circular zones form instead of denuded zones. These non-circular zones are surrounded by irregular ruptured Au islands and are covered with a fine AuSi network.*

5. A short SEM video recorded during the formation of denuded circles at 600°C is uploaded. The Au film thickness is 100nm and the time lapse is ~ 9 sec.

The video is also available online at <http://www.youtube.com/watch?v=S0L93-kU71c>